

AD-A107 289

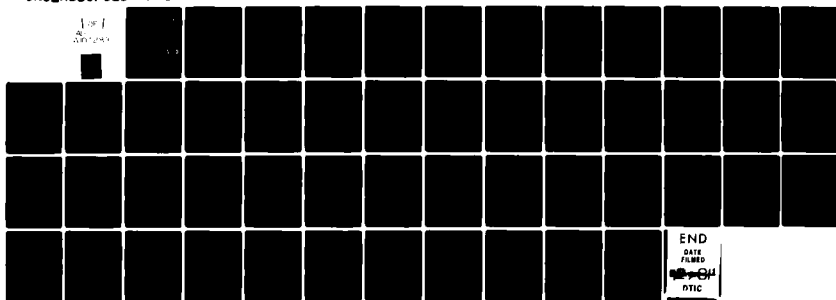
AIR FORCE INST OF TECH WRIGHT-PATTERSON AFB OH F/G 4/1
EFFICIENT RADIATIVE TRANSFER COMPUTATIONS IN THE ATMOSPHERE. (U)
JAN 81 C R POSEY

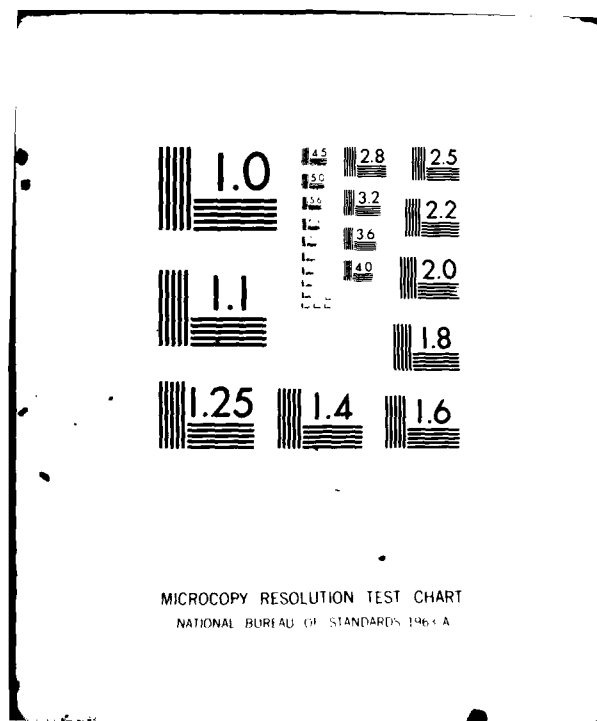
UNCLASSIFIED

AFIT-CI-81-37T

NL

For
Distribution





AD A107289

EFFICIENT RADIATIVE TRANSFER COMPUTATIONS
IN THE ATMOSPHERE

by

CHARLES ROBERT POSEY II

A.B., University of California, Berkeley
(1971)

B.S., the Pennsylvania State University,
University Park
(1975)

SUBMITTED IN PARTIAL FULFILLMENT
OF THE REQUIREMENTS FOR THE
DEGREE OF

MASTER OF SCIENCE

at the

MASSACHUSETTS INSTITUTE OF TECHNOLOGY

JANUARY, 1981

DTIC
ELECTE
NOV 16 1981

S D

Signature of Author. *Charles R. Posey II*
Department of Meteorology, January, 1981

Certified by *[Signature]*
Thesis Supervisor

Accepted by.
Chairman, Departmental Committee
on Graduate Students

DISTRIBUTION STATEMENT A
Approved for public release;
Distribution Unlimited

DTIC FILE COPY

UNCLASS

SECURITY CLASSIFICATION OF THIS PAGE (When Data Entered)

REPORT DOCUMENTATION PAGE		READ INSTRUCTIONS BEFORE COMPLETING FORM
1. REPORT NUMBER I-81-37T	2. GOVT ACCESSION NO. AD-A107 189	3. RECIPIENT'S CATALOG NUMBER
4. TITLE (and Subtitle) Efficient Radiative Transfer Computations In The Atmosphere,		5. TYPE OF REPORT & PERIOD COVERED THESIS/DISSERTATION
7. AUTHOR(s) Capt Charles Robert/Posey, II		6. PERFORMING ORG. REPORT NUMBER
9. PERFORMING ORGANIZATION NAME AND ADDRESS AFIT STUDENT AT: Massachusetts Institute of Technology		8. CONTRACT OR GRANT NUMBER(s) Master's thesis
11. CONTROLLING OFFICE NAME AND ADDRESS AFIT/NR WPAFB OH 45433		10. PROGRAM ELEMENT, PROJECT, TASK AREA & WORK UNIT NUMBERS
14. MONITORING AGENCY NAME & ADDRESS (if different from Controlling Office)		12. REPORT DATE Jan 1981
		13. NUMBER OF PAGES 38
		15. SECURITY CLASS. (of this report) UNCLASS
		15a. DECLASSIFICATION/DOWNGRADING SCHEDULE
16. DISTRIBUTION STATEMENT (of this Report) APPROVED FOR PUBLIC RELEASE; DISTRIBUTION UNLIMITED		
17. DISTRIBUTION STATEMENT (of the abstract entered in Block 20, if different from Report) APPROVED FOR PUBLIC RELEASE AFR 190-17. 16 OCT 1981 Fredric C. Lynch		
18. SUPPLEMENTARY NOTES APPROVED FOR PUBLIC RELEASE: IAW AFR 190-17 FREDRIC C. LYNCH, Major, USAF Director of Public Affairs Air Force Institute of Technology (ATC) Wright-Patterson AFB, OH 45433		
19. KEY WORDS (Continue on reverse side if necessary and identify by block number)		
20. ABSTRACT (Continue on reverse side if necessary and identify by block number) ATTACHED 81 10 27 251		

DD FORM 1 JAN 73 1473

EDITION OF 1 NOV 65 IS OBSOLETE

UNCLASS

SECURITY CLASSIFICATION OF THIS PAGE (When Data Entered)

022200

EFFICIENT RADIATIVE TRANSFER COMPUTATIONS IN
THE ATMOSPHERE

by

CHARLES ROBERT POSEY II, CAPT, USAF

Submitted to the Department of Meteorology,
Massachusetts Institute of Technology in January 1981 in
partial fulfillment of the requirements for the degree of
Master of Science.

ABSTRACT

An efficient longwave radiation transfer band model was developed and applied to the MIT Stratospheric General Circulation Model (GCM). The band model is a revised version of models by Ramanathan (1976) and by Alimandi and Visconti (1979). It is validated by comparison with work by Dopplack (1971), Slade (1969) and by Park and London (1974).

The band model produced pole-to-pole heating gradients up to 9 degK/day compared with Newtonian heating gradients of 1-2 degK/day used previously in the GCM. In 5 day model integrations, the band model sharpened erroneous temperature gradients in the GCM when compared with the Newtonian heating scheme. Poleward eddy heat fluxes appear to be too weak in the low-resolution, 6 wave spectral GCM to balance the heating gradients of the band model. An 18-wave spectral GCM is planned by the MIT stratospheric working group.

With the band model, global heating rates up to 3 degK/day are noted. Such global heating rates cannot be sustained in the atmosphere. Methods to achieve global heating balance are explored. The most straight forward method is to set the horizontal-averaged temperatures of the GCM equal to the radiative equilibrium temperatures of the band model.

Thesis Advisor: Dr. Ronald G. Prinn, Associate Professor of
Meteorology and Physical Oceanography

TABLE OF CONTENTS

	Page No.
ABSTRACT.	2
LIST OF FIGURES	4
LIST OF TABLES.	5
1. INTRODUCTION	6
2. RADIATION THEORY AND THE RAMANATHAN/ VISCONTI BAND MODEL.	8
3. CODE EFFICIENCY IMPROVEMENTS	14
4. VALIDATION OF THE REVISED BAND MODEL	18
5. DIABATIC HEATING IN THE MIT STRATOSPHERIC GCM.	21
6. SUMMARY.	32
ACKNOWLEDGMENTS	35
REFERENCES.	36
FIGURES	38

Accession For	
NTIS GRA&I	<input checked="" type="checkbox"/>
DTIC TAB	<input type="checkbox"/>
Unannounced	<input type="checkbox"/>
Justification	
By	
Distribution/	
Availability Codes	
Dist	Avail and/or Special
A	

LIST OF FIGURES

- Figure 1: $15\mu\text{CO}_2$ cooling rates (degK/day).
- Figure 2: $9.6\mu\text{O}_3$ cooling rates (degK/day).
- Figure 3: Net diabatic heating rates.
- Figure 4: UV heating rates.
- Figure 5: CO_2 cooling rate sensitivities to a 5°K temperature perturbation at selected model levels.
- Figure 6: MIT GCM zonal averaged temperatures, Day 361, Run 34.
- Figure 7: Zonal averaged net diabatic heating rates with Newtonian cooling, Day 361, Run 34.
- Figure 8: Zonal averaged net diabatic heating rates with band model cooling, Day 361, Run 34.
- Figure 9: Zonal averaged net diabatic heating rates with adjusted cooling, Day 361, Run 34.
- Figure 10: Zonal averaged temperature field after 5 days model integration with Newtonian cooling.
- Figure 11: Zonal averaged temperature field after 5 days model integration with band model cooling.
- Figure 12: Zonal averaged vertical velocities ($\text{mb/sec} \times 10^7$) after 5 days model integration with Newtonian cooling.
- Figure 13: Zonal averaged vertical velocities ($\text{mb/sec} \times 10^7$) after 5 days model integration with band model cooling.

LIST OF TABLES

	Page No.
TABLE 1.: Code Efficiency Improvements.	16
TABLE 2.: Heating Components in the Newtonian Five Day GCM Run at 80°N.	26
TABLE 3.: Heating Components in the Band Model Five Day GCM Run at 80°N.	27
TABLE 4.: Global Model Heating Rates.	29
TABLE 5.: Band Model Radiative Equilibrium Temperatures and GCM Global Average Temperatures.	31

1. INTRODUCTION

A numerical simulation of the general circulation must assume some knowledge of the diabatic sources and sinks of heat energy. How much detail of the radiative energy distribution can be included in a particular general circulation model (GCM) depends on the problem considered, the accuracy desired and the runtime constraints required. This paper addressed the need for efficient radiative transfer computations in the stratosphere and mesosphere when accurate simulation is sought under runtime constraints.

Murgatroyd and Goody (1958) presented one of the first summaries of net diabatic heating rates due to radiation in the stratosphere and mesosphere. Dopplnick (1971), Slade (1969), and Tahnk and Newell (1975) have reported heating rates due to the major stratospheric absorbing gases, CO_2 and O_3 , using automated radiation band models. Park and London (1974) include the minor stratospheric gas, H_2O . Dickinson (1972) made revisions to the CO_2 band model by including the effects of minor isotopic and "hot" bands.

Leovy (1964) developed theoretical dynamical models for the upper atmosphere based on an idealized, symmetrical version of the radiative heating distribution. Manabe and Hunt (1968) incorporated radiative band models into a stratospheric general circulation model up to 40 km. Dickinson (1973) addressed the need for rapid radiative computations for use in GCMs, suggesting a Newtonian cool-to-space

approximation for infrared cooling. This method takes negligible computation time but neglects layer-to-layer exchanges of heat.

Ramanathan (1976) reported a radiative transfer band model which he claimed to be an order of magnitude faster than the detailed radiative models by Dickinson (1972) and Ellingson (1972) and yet accurate to within 1% of their results. In 1978-79 Visconti (1979) modified the long wave radiation portions of the Ramanathan model for the gases CO_2 and O_3 . The purpose of the work reported here is to further streamline this radiative transfer code and incorporate it into the MIT stratospheric general circulation model where it replaces a Newtonian cooling-to-space scheme.

To date, the computation time for CO_2 has been reduced by a factor of 20. The ozone computation time has been reduced by a factor of two. These two components have been applied to the GCM above 30 km. Net radiative heating rates compare well with Park and London (1974). Increases in magnitude up to a factor of 6 in the pole-to-pole heating gradient are found in comparison with the Newtonian cooling approximation.

The MIT GCM predicts a temperature gradient directed from the winter pole to the summer pole at 70 km in contrast with observations. The initial effect of the more realistic radiative heating rates is to sharpen the winter-summer

gradient in the model.

Horizontally-averaged heating rates up to +3 deg/day (30% of the maximum pole to pole differential heating) are found at upper atmospheric levels. This net heat imbalance appears because the band model radiative equilibrium temperature profile is warmer than the reference temperature profile of the GCM. An empirical parametrization of sub-grid scale vertical eddy heat diffusion is presented as one method to accommodate the heat imbalance.

2. RADIATION THEORY AND THE RAMANATHAN/VISCONTI BAND MODEL

In the long wave range of the electromagnetic spectrum, radiant energy is produced by emission everywhere in the atmosphere. For a given frequency, ν , the flux of radiant energy at a point is the integral of the emitted energy from every point in the atmosphere attenuated according to Beer-Lambert's Law of exponential decay through absorption by the intervening absorbing gases. Long wave cooling, Q , is the result of a divergence of this three dimensional flux. (See, for more detail, Goody, 1964)

$$Q_{\nu} = \frac{-\nabla \cdot F_{\nu}}{\rho c_p} \quad (1)$$

ρ = density

c_p = constant pressure heat capacity

Atmospheric band models generally simplify the geometry of radiative transfer by assuming a vertically stratified plane parallel atmosphere with horizontally homogeneous temperature and absorber gas compositions at each grid point considered. Integration over zenith angle can be parameterized in the plane parallel atmosphere with a constant "diffusivity" factor so that the problem is reduced to one dimension:

$$Q_v = - \frac{1}{\rho c_p} \frac{dF_v}{dz} \quad (2)$$

Rodgers and Walshaw (1966) compiled evidence that the cooling rate error due to using a constant diffusivity is 1.5 per cent or less when compared with more complex transmission dependent zenith-integrated diffusivities.

In the Ramanathan model, the carbon dioxide 15μ band and the ozone 9.6μ band are each handled by empirically derived band absorptance formulations, in which a mean absorptance for an entire band is defined for a given atmospheric path based on temperatures, pressures, and absorbing gas amounts along the path together with other predetermined parameters.

Following Manabe and Möller (1961), the appropriate version of the radiative transfer equation for $F(z)$, the net flux at a given level, is obtained by integrating the basic equation (3) vertically from the ground to level z

and then from the top of the atmosphere to level Z with black body radiation at the ground and no downward radiation at the top of the atmosphere.

$$\frac{dI(Z')}{d\tau} = I(Z') - J(Z') \quad (3)$$

where I is the radiation intensity along a path
 J is the source function for emission and
 τ is the optical depth

Using the Planck function, B , as the source function, multiplying by the integrating factor, $\Gamma = e^{-\tau}$, and integrating by parts gives the upward flux, $I_{\uparrow}(Z)$ and downward flux, $I_{\downarrow}(Z)$:

$$I_{\uparrow}(Z) = B(Z) + \int_Z^{Z_{\text{sfc}}} \Gamma(Z'-Z) dB$$

$$I_{\downarrow}(Z) = B(Z) - B(Z_{\text{top}}) \Gamma(Z_{\text{top}}-Z') + \int_Z^{Z_{\text{top}}} \Gamma(Z'-Z) dB \quad (4)$$

Introducing the absorptance, $A = 1 - \Gamma$, the net flux at level Z is given by equation (5)

$$\text{Net Flux, } F(Z) = I_{\uparrow} - I_{\downarrow} = B(Z_{\text{sfc}}) - B(Z_{\text{top}}) A(Z_{\text{top}}, Z) - \int_{Z_{\text{top}}}^{Z_{\text{sfc}}} A(Z', Z) dB(Z') \quad (5)$$

where $A(Z', Z)$ represents the absorptance between level Z' and level Z .

The above expression is exact when applied to a single wave frequency. When equation (5) is applied to a band, the absorptance must be parameterized empirically. Equations (2) and (5) are the basic cooling rate and flux computation equations used in the Ramanathan model.

The $15\mu\text{CO}_2$ and $9.6\mu\text{O}_3$ bands are sufficiently narrow that a single wave frequency can be used to evaluate the Planck function: 667 cm^{-1} for CO_2 and 1041 cm^{-1} for O_3 .

The empirical absorptance formulations developed by Cess and Tiwari (1972) are used by Ramanathan. For carbon dioxide, the pressure-broadened absorptance is given by

$$A(\zeta) = 2A_0 \ln \left\{ 1 + \sum_{i=1}^{10} \zeta_i^{\frac{1}{2}} \right\} \quad (6)$$

$$\text{where } \zeta_i = 1.66 \left(\frac{4\nu_0}{A_0 D_i} \right) \int S_i q_i P_c P dZ$$

ν_0 = mean line half width spacing

A_0 = band width parameters

q_i = relative abundance of isotopes to the primary isotope

D_i = mean line spacing

S_i = band intensity

P_c = partial pressure of carbon dioxide

P = atmospheric pressure

where four isotopic and six "hot" bands are considered. A strong line approximation has been used.

Alimandi and Visconti (1979) achieved a reduction in computation time by noting that the band width parameter, A_o , may be scaled as $A_o = 22.3 \text{ cm}^{-1} (T/300)^{1/2}$ so that A_{ij} , the absorptance between two pressure levels i and j , can also be scaled like the square root of temperature at the lower level, i .

$$A_{ij} = A_{ij}^{\text{ref}} (T_i/T_i^{\text{ref}})^{1/2} \quad (7)$$

The band absorptance formula for Doppler broadening used by Ramanathan is shown in equation (8).

$$\begin{aligned} A(u) &= A_o u (1 - 0.18u/\delta) \quad u/\delta \leq 1.5 \quad (8) \\ &= 0.753 A_o \delta \{ [\ln(u/\delta)]^{3/2} + 1.2 \} \quad u/\delta > 1.5 \end{aligned}$$

where $\delta = K v_d$

v_d = Doppler line half width

u = optical path length

$$= \frac{S}{A_o} P_c$$

Both the doppler half width, v_d , and the band width parameter, A_o , are proportional to the square root of temperature so for $u/\delta > 1.5$, doppler absorptance scales like temperature:

$$A_{ij} = A_{ij}^{\text{ref}} (T_i / T_i^{\text{ref}}) \quad (9)$$

Alimandi and Visconti's version of the CO₂ band model computes Doppler and Lorentz absorptances for a reference temperature profile and uses the scaling described to compute absorptances for each new temperature profile. Using a seasonal and latitudinal range of temperature profiles, Alimandi and Visconti (1979) found accuracy remained within 10% of the exact computation when the scaling was used.

For ozone, the strong line approximation is not valid in the atmosphere. Therefore a more complex band absorptance formulation must be used for pressure broadening. Also, ozone mixing ratios vary with season and, above 60 km, even diurnally. For these reasons, scaling was not feasible in the O₃ band model and the absorptances were calculated for each profile using equation (10).

$$A(u, \beta) = 2A_o \ln \left\{ 1 + \frac{u}{[4 + u(1 + 1/\beta)]^{1/2}} \right\} \quad (10)$$

where the line width parameter, $\beta = \frac{4v_o}{uD} \int P du$
and all other symbols have been defined in equations (6) and (8).

3. CODE EFFICIENCY IMPROVEMENTS

Radiative transfer is inherently a time consuming computation. To take account of exchange of radiative energy between the layers of the atmosphere in an n - layer model requires that code be repeated at least $n \times n$ times. In fact greater vertical resolution may be required. To use the Ramanathan band absorptance formulation required a vertical resolution of better than 3 km. For the MIT 26 level, 0-72km stratospheric GCM that meant the flux computation code was repeated $2 \times n \times n$ (1352) times for a single profile.

The second feature of radiative transfer code which makes it time consuming is the necessity of using mathematical functions such as the exponential, logarithm and square root functions. The exponential is required for the Planck function of a single frequency. In Ramanathan's band absorptance formulation both natural logarithm and square root are required.

Efficiency improvements are made by concentrating on the features of repeated code and mathematical functions. Table 1 lists the results of improvements made in average run time for one time step on December 1 in the MIT Stratospheric GCM. The band model heating code is used at 240 grid points for incorporation into the six-wave, spectral GCM.

For the CO_2 code the first improvement was to compute

and table the Planck function $B = \frac{a}{e^{b/T-1}}$ and scaling factors $T_i/T_{i,ref}, [T_i/T_{i,ref}]^{1/2}$ for each layer of the band model. Computation time dropped by a factor of six with no loss of accuracy. (See Table 1, Section 1.)

The second improvement relied on a feature of the CDC computer hardware. In the CDC central processor, the instruction word stack (IWS) holds up to 48 instructions. If a do loop will fit completely in the IWS, computation is much more efficient since instructions need not be fetched from memory in each repetition of the loop. For the CO₂ flux computation, separating the upward and downward flux components resulted in two do loops each of which could fit in the IWS. Because the flux computation dominates the code time, an overall speed-up factor of two was achieved, still with no loss of accuracy.

Finally, tables of the Planck function and square root were prepared as functions of temperature in the range of 150-350° K. The tables were computed for every degree Kelvin. The square root table gave values with .1% accuracy without interpolation. The Planck function was accurate within 1% using linear interpolation. A further reduction in speed of 30% was achieved. Heating rates remained accurate within .1 deg/day.

For the O₃ code, precomputing the Planck and square root functions of temperature resulted in speeding the code by a factor of 2. (See Table 1, Section 2.) This was not

TABLE 1.: Code Efficiency Improvements

		GCM Runtime (sec)	Band Model Runtime (sec)
1.a.	Unaltered CO ₂ code	13.35	11.28
1.b.	Precomputing Planck function and scaling factors	3.96	1.89
1.c.	Instack do loops	2.92	.85
1.d.	Tabling EXP/SQRT values	2.72	.65
2.a.	Unaltered O ₃ code	23.47	21.40
2.b.	Precomputing Planck function and SQRT of temperature	11.44	8.72
2.c.	Calculating once a day	2.43	.36
3.a.	Unaltered GCM	2.07	--
3.b.	GCM with unaltered CO ₂ and O ₃ code	34.75	32.08
3.c.	GCM with revised CO ₂ and O ₃ code	3.08	1.13

as large as the effect in the CO_2 code. The primary reason it was not as effective here was because the band absorptance calculation still required a logarithm and square root to be performed at each level of the flux computation. If tables of these functions could give sufficient accuracy another factor of two could be realized.

Even if tables were successful the total GCM runtime would be doubled by the O_3 code alone. Since ozone 9.6μ cooling is never greater than 20% of the CO_2 cooling and is not subject to rapid variation, less frequent calculation could be justified. In the run described in later sections ozone cooling was calculated once a day and its effect was smoothed over 24 hours to prevent discontinuities. This was effectively a drop in runtime by a factor of 24.

The unaltered radiation code overwhelmed the GCM runtime by a factor of 10. The described revisions fit the infrared radiation code into 30% of the total runtime.

The dominance of the flux computation in the band model was clear. In the fastest CO_2 code, the flux computation involved only five multiplications, a conditional branch, and three additions for each layer-exchange. Still, the flux computation took 92% of the CO_2 band model time (.6 sec/.65 sec per time step). Thus speeding other portions of the code by more efficient indexing, identifying invariant code, and other optimizations did not lead to

significant improvements overall. Further major improvements will require a reduction in the number of layer exchanges considered at each time step in the flux computations.

A sensitivity analysis was performed for an isolated 5° temperature rise at each level of the model. Results are summarized in Figure 5 for typical levels. Cooling rate changes of more than .1 deg/day occurred at the level perturbed and at the next higher level from the ground to 27 km. Above 27 km, .1 deg/day changes or greater were found at not more than six levels: one level below to four levels above the perturbed level. Thus layer to layer exchange need only be computed at six layers on an hour to hour basis. Flux contributions from other levels can be calculated less frequently and stored. Another factor of 5 in computation speed would be saved by dropping from 52 half levels to 12 half-levels contributing to calculations, but a baseline of the time-integrated affects of the current revision of the model should be set first.

4. VALIDATION OF THE MODEL

For validation of the revised radiative band model, I used ozone and temperature analyses given by Park and London (1974). Since their temperature profile does not extend to the surface, I also used temperatures from Kuhn and London (Fig. 3, 1969). For near surface ozone amounts,

I used values from an MIT GCM run. Park and London do not report CO_2 and O_3 cooling separately so to examine these components I have compared them with results from Dopplnick (1971) and Slade (1969). In Figure 1, $15\mu\text{CO}_2$ cooling rates are given. In agreement with Dopplnick and Slade the analysis shows maximum cooling at the stratopause in the summer data. Warming occurs near the equatorial tropopause and in the summer data at 70 km. One difference is that the revised Ramanathan model also finds warming throughout the data below 3 to 8 km. When applied in the MIT GCM the Ramanathan model will not be used in the troposphere.

In Figure 2, $9.6\mu\text{O}_3$ cooling rates are displayed. Maximum cooling is centered on the stratopause and extends to all but the winter polar night latitudes. Warming is found throughout the lower stratosphere. In both regions the Ramanathan model gives weaker effects than the Dopplnick and Slade models up to 1 degK/day. Considering differences in the temperature profiles used, agreement is fairly good.

Combining the CO_2 and O_3 band model with the MIT GCM UV heating code resulted in the net heating rates shown in Figure 3. July data is presented on the left of the figure to match the published data by Park and London (1974). IN the summer hemisphere on both analyses, heating peaks at 10 deg/day at 50 km in the polar region. A ridge of strong heating extends towards the equator sloping downwards to 40 km. This secondary maximum is stronger in results

based on Ramanathan's code.

In the winter hemisphere, maximum cooling is at 60 km. Park and London have a higher maximum cooling (-10 deg/day vs. -7 deg/day). The major difference in the analysis structure appears to be the extension of the cooling rate "trough" at 60 km southward across the analysis in Figure 3. Park and London's data do not show a feature like this.

Figure 4 is an analysis of the GCM UV heating rates. Comparison with Park and London's UV heating rates shows that the equatorial cold trough and enhanced 65-70 km heating in the summer hemisphere are due to differences in the UV heating rates. These in turn are probably because the published ozone analysis is for daytime amounts while the net UV rates published were integrated around the 24 hour cycle during which ozone amount can vary substantially especially at high altitudes.

The greater cooling in the winter hemisphere seen by Park and London is due at least in part to the inclusion of cooling by the $80 \mu\text{H}_2\text{O}$ band. Kuhn and London (1969, Fig. 8) show radiative cooling rates up to -1 deg/day for a water vapor mixing ratio of 10^{-6} in the upper atmosphere. They consider 10^{-6} the most probable value. Estimating numerical values from the published temperature and ozone analyses is another source for differences.

5. DIABATIC HEATING IN THE MIT STRATOSPHERIC GCM

The MIT Stratospheric General Circulation Model was designed by Cunnold et al. (1975) to simulate ozone production and transport. Since seasonal ozone amounts are irregular, several years of integration are required to reach a statistically steady state. This requirement led to the choice of a dynamic "balance" equation system (Lorenz, 1960) which can accept a time step up to an hour.

The thermodynamic prediction equation for this system is given in equation (11) in the form used in the GCM:

$$\frac{\partial T'}{\partial t} = -k \times \nabla \Psi \cdot \nabla T' - W \left(\frac{dT_s}{dz} + \frac{RT_s}{C_p} \right) + \frac{q'}{C_p} \quad (11)$$

$T_s(z)$ = is the standard atmospheric reference temperature profile

T' = deviations from T_s

Ψ = stream function for horizontal velocity

$z = -\ln(p/1000\text{mb})$

$W = \frac{dz}{dt}$

q' = diabatic heating per unit mass minus its horizontal global average

In this equation, only deviations from the reference temperature profile are predicted. To assure conservation of energy, average temperature on a model level is not allowed to vary. On each level, the static stability

parameter is held constant. Any net imbalance in the global diabatic heating rate for a level is removed equally at all gridpoints. These features can potentially distort the radiative-dynamical coupling. Cunnold et al. (1975) justify these approximations as not affecting significant conclusions about ozone while allowing great improvements in computational efficiency.

Diabatic heating, q , is determined empirically in the troposphere so as to reproduce known seasonal estimates of q using observed seasonal distributions of temperature. No attempt was made in this work to alter this portion of the heating code.

In the upper atmosphere, absorption of solar radiation by ozone is computed explicitly as the product of the solar constant, I_λ , times the absorption coefficient of ozone, σ_λ , ozone mixing ratio and the transmission function, $e^{-\tau_\lambda}$, all integrated over wavelength in the solar spectrum. Infrared cooling is parameterized with a first term Taylor approximation about the $15\mu\text{CO}_2$ cooling rates for the 1962 temperature reference profile. The cooling coefficients used are due to Dickinson (1973). This approximation is represented as Newtonian cooling-to-space because it depends only on the local temperature. Radiational exchange with other levels only appears in the exact cooling rates of the reference profile. Because this scheme is linear in temperature, the calculation could

be done in spectral coordinates very rapidly. However, it is known to be inexact up to a factor of 2 at 70 km even when non-linear pressure and temperature corrections are included. (See Dickinson, 1973, Figure 4.)

The streamlined Ramanathan band model was introduced into the model in grid format immediately following the UV heating calculation which is also done in grid format. Conversion to spectral form for use in the prediction equations is done using a fast fourier transform. Spectral representation leads to errors up to 1 degK/day especially for the UV heating. UV heating rates resemble a step function at the edge of the polar night before spectral smoothing and are therefore hard to represent.

Figure 6 displays an analysis of model temperatures for December 1 at the beginning of the second year of RUN 34 in the MIT stratospheric GCM. In comparison with the analysis of observed temperature of Park and London (1974), the model analysis shows temperatures which are too cold throughout the polar region above 20 km. This feature has been typical of most GCMs. Figures 7 and 8 show the net heating rates on December 1 using respectively, Newtonian cooling and the revised Ramanathan band model. The global mean heating has been removed at each level so these figures show the values, q/c_p , used in the prediction equation (11). In Figure 7 cooling rates are generally small. Newtonian cooling appears to match closely the UV

heating everywhere. Heating is strongest in the equatorial stratopause region. Cooling is strongest in the polar night except at 40 km where warming occurs at the temperature minimum. By contrast, Figure 8 shows an eight degree pole-to-pole gradient at 55 km primarily due to stronger radiative cooling in the polar night.

Figures 10 and 11 show the effects of 5 days model integration on the model temperature field by the two cooling schemes. Comparing Figures 6 and 10 the Newtonian cooling scheme shows a 5 degree warming at the top of the model in the winter polar region. By equation (11) this appears must be due to horizontal advection of heat since there is weak radiative and adiabatic vertical motion cooling in this region (see Figures 7 and 12) throughout the period. At 40 km at the winter pole there has been 6 degree warming smoothing the temperature minimum found there at slightly less than the diabatic heating rate of $1^{\circ}\text{K}/\text{day}$. There is a major 20°K cooling in the summer troposphere at 200 mb in both integrations, but the radiative cooling rates are much too weak to have played a major role there.

In Figure 11 after 5 days GCM integration using the Ramanathan model there is little change in temperature in the winter polar region at the top of the GCM. In comparison with the Newtonian model run, radiative cooling is greater in the Ramanathan model. This greater cooling

counteracts the horizontal heat convergence noted above. At the temperature minimum at 40 km the temperature has slipped four degrees to an even colder value. In both regions the band model radiational cooling has increased the anomalous pole-to-pole temperature gradient in comparison with the Newtonian scheme.

One effect of radiational cooling which could be expected would be a compensatory adiabatic warming by sinking motions. Figures 12 and 13 show the zonal average vertical velocities field found in the model after 5 days with the two radiation schemes. There are no significant differences in the two fields suggesting that the adiabatic warming induced by the increased radiational cooling in the winter polar region is negligible. The vertical velocities are, in fact, upward suggesting that the major energy balance is between horizontal advection of heat and the adiabatic cooling by the vertical velocities which are fairly steady over the 5 day period above 30 km. In Tables 2 and 3 are the magnitudes of the terms of the thermodynamic prediction equation for the upper atmosphere. Horizontal heat advection was computed as a residual from the other components. The major balance terms are the horizontal influx of heat by advection and the adiabatic cooling by rising vertical motions. Comparison of the two tables suggest that, at least in the initial 5 day period the increased cooling by the band model over the Newtonian

TABLE 2.: Components of the Thermodynamic Heating in the
Newtonian Five Day Model Run at 80°N (degK/day).

Height	Model Level	$-\frac{\partial T}{\partial t}$	$= -k \times \nabla \Psi \cdot \nabla T$	$-\frac{dz}{dt} \sigma$	$+\frac{q'}{C_p}$
70km	2	1.1	12.6	-10.9	- .6
	3	1.2	21.3	-18.6	-1.5
	4	1.0	26.9	-24.1	-1.8
60km	5	1.1	31.6	-28.5	-2.0
	6	1.1	32.0	-28.6	-2.3
	7	1.1	31.0	-27.4	-2.5
50km	8	1.1	29.7	-26.4	-2.2
	9	1.5	33.2	-29.5	-2.2
	10	1.6	26.9	-23.9	-1.4
40km	11	1.1	20.3	-19.4	.2
	12	1.4	14.7	-13.5	.2
	13	1.9	13.0	-10.4	- .7
30km	14	1.1	10.5	- 8.4	-1.0
	15	-.7	7.0	- 6.5	-1.2
	16	+.8	7.5	- 4.7	-2.0
25km	17	.0	5.4	- 3.6	-1.8

TABLE 3.: Components of the Thermodynamic Equation in the Band Model Five Day GCM Run.

Height	Model Level	$\frac{\partial T}{\partial t}$	$= -k \times \nabla \Psi \cdot \nabla T$	$-\frac{dz}{dt} \sigma$	$+\frac{q'}{C_p}$
70km	2	+ .2	12.4	- 9.7	-2.5
	3	- .1	20.2	-16.8	-3.5
	4	- .6	26.7	-23.5	-3.8
60km	5	- .6	31.9	-27.7	-4.8
	6	-1.4	33.1	-28.2	-6.3
	7	-1.3	32.2	-27.4	-6.1
50km	8	-1.2	30.9	-26.7	-5.4
	9	- .1	34.5	-30.3	-4.3
	10	- .2	28.2	-24.6	-3.8
40km	11	- .9	22.1	-20.3	-2.7
	12	- .6	15.2	-14.1	-1.7
	13	+ .7	12.2	-10.4	-1.1
30km	14	- .7	9.4	- 8.2	-1.9
	15	-1.3	7.4	- 6.7	-2.0
	16	+ .6	7.2	- 5.0	-1.6
25km	17	+ .3	5.7	- 3.6	-1.8

scheme primarily affects the local temperature change. The difference in the local temperature changes between the model runs is roughly 10% of the horizontal heat advection term.

There is some dynamical adjustment to the increased radiational cooling even in the five day model run. For example, at level 9 near the stratopause the horizontal and vertical adiabatic terms produced 4.2 deg K/day heating with the band model. This was .5 deg K/day stronger than in the Newtonian run. This reflects an increase in circulation intensity with a negative feedback on the increased radiational cooling in effect. Longer model runs will be needed to determine the final extent of the dynamical adjustment and the final effects on the meridional temperature gradient.

Manabe and Hunt (1968, Fig. 17) determined heat balance components in an 18 level stratospheric general circulation model up to 37.5 km. At 79°N, heat was added by large scale eddies. Heat was lost by the mean meridional circulation (MMC) and radiative effects in a 2:1 ratio above 25 km in their model. Table 3 suggests qualitative agreement with Manabe and Hunt. Vertical velocities are weaker in Manabe and Hunt's model in the 25-40 km range. This is probably because these levels are near the rigid upper lid in their model.

As mentioned in the discussion of the thermodynamic

TABLE 4.: Global Model Heating Rates

Height	Level	Net	UV	15 μ CO ₂	9.6 μ O ₃	UV (in balance)
70km	1	-	-	-1.44	.15	-
	2	-.01	2.24	-2.35	.10	2.25
	3	.27	3.08	-2.85	.04	2.81
60km	4	.88	4.29	-3.33	-.09	3.41
	5	1.75	5.74	-3.66	-.33	3.99
	6	2.46	7.06	-3.85	-.75	4.60
	7	1.76	8.05	-4.84	-1.45	6.29
50km	8	1.89	9.44	-5.49	-2.07	7.55
	9	2.22	10.68	-6.83	-1.64	8.47
	10	3.15	10.44	-5.78	-1.51	7.29
	11	2.84	8.50	-4.73	-.94	5.67
40km	12	1.41	5.90	-3.91	-.58	4.49
	13	.30	4.08	-3.16	-.63	3.79
	14	.10	2.91	-2.47	-.33	2.81
30km	15	.49	2.17	-1.61	-.07	1.69
	16	.76	1.59	-1.07	.24	.83
	17	.77	1.05	-.72	.44	.28
20km	18	.50	.59	-.52	.43	.10
	19	.16	.27	-.37	.26	.11
	20	.21	.09	-.12	.12	.00
	21	.10	.04	-.09	.05	.04
	22	.02	.01	-.11	.01	.10

prediction equation, net imbalances in the horizontal global heating rates are effectively subtracted out at all grid points. These net imbalances are not small at some levels. Table 4 shows the net global heating averages for the Ramanathan model heating rates in Figure 8. The maximum value occurs at level 10: + 3.15 deg K/day. The model equations require that this be subtracted out before entry into the prediction equation. So, at the winter pole, infrared cooling computed as +.31 became -3.76 when the global heating was subtracted. The additional error of $-.92^{\circ}\text{K}$ is due to spectral smoothing of the UV heating.

Net global radiative heating in the upper atmosphere has been noted by other authors. Johnson and Gottlieb (1971) computed vertical eddy heat diffusion coefficients as a function of altitude based on the assumption that the excess global heating diffuses to lower atmospheric levels where the increased densities make it negligible. In the spectral coordinates a simple way to represent this diffusion would be to adjust the UV heating components proportionally to balance the global infrared cooling as shown in Table 4. at each model level:

$$Q'_{uv} = Q_{uv} \cdot \left| \frac{\bar{Q}_{\text{CO}_2} + \bar{Q}_{\text{O}_3}}{\bar{Q}_{uv}} \right| \quad (12)$$

Net global heating exceeds 1 deg/day between 40 and 60 km as shown in Table 4. In this range, the adjustment

TABLE 5.: Band Model R.E. Temperatures and GCM Global Average Temperatures.

Model Level	Approx. Height (km)	Radiative* Equilibrium Temperatures	Global Average Temperatures
1	72	242	211
3	66	248	227
5	61	263	242
7	55	276	259
9	48	282	267
11	42	260	255
13	36	238	243
15	30	226	231
17	25	220	220
19	20	216	212
21	15	220	213
23	9	236	234
25	3	276	266

* Alimandi and Visconti (1979)

factor in (12) was fairly constant, ranging from .65-.79.

An analysis of net diabatic heating rates using this adjustment is shown in Figure 9. In comparison with Figure 8, the unadjusted band model heating rates, the general shape of the heating analysis appears to be preserved but the magnitude of the gradients has been reduced.

Net global heating was found at essentially all model levels in the upper atmosphere. The radiational band model is trying to heat the entire atmosphere in this region. Alimandi and Visconti (1979) have calculated a radiative equilibrium temperature profile for their version of the band model. Since the band model reported here is based on theirs, their equilibrium profile should apply at least approximately. Table 5 showed that at almost all levels, the radiative equilibrium temperature is warmer than the specified horizontal average temperatures of the GCM. The GCM horizontal average temperatures are based on observations, but the upper atmosphere observations are not considered highly reliable. A straight forward method of tuning the models into agreement would be to use the radiative equilibrium temperatures as the specified horizontal average temperatures in the GCM.

6. SUMMARY

The revised Ramanathan band model developed in this work appears to be in good agreement with the work of

Dopplnick (1971), Slade (1969), and Park and London (1974), while being much faster than the original code.

When incorporated into the MIT stratospheric GCM, the band model created much stronger pole-to-pole differential heating than the Newtonian heating scheme. After only a five day period of integration, the band model sharpened the existing erroneous temperature gradients by several degrees. However it was noted that the differences in local temperature changes between the heating schemes are only 10% of the horizontal heat advection. Poleward horizontal eddy heat fluxes tend to increase with increasing resolution in GCMs. Thus when the MIT stratospheric model is converted from six to eighteen wave resolution, the band model may handle heating more accurately than the Newtonian model. Dynamical time constants are longer than five days and some dynamical adjustment was noted. Longer model runs will be appropriate in the eighteen wave GCM to determine steady state average heating rates and meridional temperature gradients.

The existence of large net global heating rates, especially from 40-60 km, was identified as a problem in applying the radiation band model to the balance equations of the MIT stratospheric GCM. To adjust the UV heating alone would require a 20-35% reduction in UV heating in the 40-60 km region. A more general procedure to bring the band model into balance in the GCM would be to use the

(band model radiative equilibrium temperatures to specify
the horizontal average temperatures of the GCM.

ACKNOWLEDGMENTS

I have greatly appreciated my advisor, Dr. Ronald Prinn for his insight and guidance. Dr. Reginald Newell has been most helpful with data and ideas. I would like to thank Drs. Derek Cunnold and Fred Alyea and Mr. Carlos Cardelino for their assistance with the MIT Stratospheric GCM. I am grateful to Mike Kirkish for breaking me in on the CDC 7600 and to Amram Golembek for his help and companionship.

I acknowledge gladly a debt of appreciation to Dr. Guido Visconti for making his radiation band model programs available to me and for his aid in using them.

I will remember Liz Manzi appreciatively for her skilled typing and our conversations.

The patience and support my wife Denise has given me has meant a great deal to me.

My master's program was made possible through the Air Force Institute of Technology.

REFERENCES

1. Alimandi, G. and G. Visconti, 1979; Thermal Structure and Relaxation Rates of the Perturbed Atmosphere: A Study with a Photochemical Radiative Convective model. Il nuovo Cimento, Vol. 2, No. 2., pp 187-208.
2. Cess, R.D. and S.N. Tiwari, 1972; Infrared radiative energy transfer in gases. Advances in Heat Transfer, Vol. 8, Academic, 229-283.
3. Cunnold, D., F. Alyea, N. Phillips and R. Prinn, 1975; A three dimensional dynamical-chemical model of atmospheric ozone, J. Atmos. Sci., 32:170-194.
4. Dickinson, R.E., 1972; Infrared radiative heating and cooling in the venusian mesosphere. 1: Global mean radiative equilibrium. J. Atmos. Sci. 29, 1531-1556.
5. _____, 1973; Method of parameterization for infrared cooling between altitudes of 30 and 70 kilometers. J. Geophys. Res., 78, 4451-4457.
6. Dopplick, T.G.; Global heating of the Earth's atmosphere, MIT Planetary Circulation Project, Report No. 24 (1971).
7. Ellingson, _____, 1972; A new longwave radiative transfer model: Calibration and application to the tropical atmosphere. Ph.D. thesis, Florida State University.
8. Goody, R.M., 1964; Atmospheric Radiation. Oxford University Press.
9. Johnson, F.S., and B. Gottlieb, 1970; Eddy mixing and circulation at ionospheric levels. Planet. Space Sci., 18, 1707-1718.
10. Kuhn, W.R. and J. London, 1969; Infrared radiative cooling in the middle atmosphere (30-110 km). J. Atmos. Sci. 26, 189-204.
- 11a. Leovy, C., 1964a; Radiative equilibrium of the mesosphere. J. Atmos. Sci., 21, 235-248.
- 11b. _____, 1964b; Simple models of thermally driven mesospheric circulation. J. Atmos. Sci. 21, 327-341.
12. Lorenz, E., 1960; Energy and numerical weather prediction. Tellus, 12, 364-373.
13. Manabe, S. and F. Möller, Dec. 1961; "On the Radiative Equilibrium and Heat Balance of the Atmosphere,"

Monthly Weather Review, Vol. 89, No. 12, pp. 503-532.

14. Manabe, S. and B.G. Hunt, 1968; Experiments with a stratospheric General Circulation Model I, Radiative and Dynamic Aspects, Mon. Wea. Rev., Vol. 96, No. 8, pp. 477-502.
15. Murgatroyd, R.J., and R.M. Goody, 1958; Sources and sinks of radiative energy from 30 to 90 km. Quart. J. Roy. Meteor. Soc., 84, 225-234.
16. Park, J.H. and J. London, 1974; Ozone Chemistry and Radiative Heating of the Middle Atmosphere, J.A.S., Vol. 31, pp. 1898-1916.
17. Ramanathan, V., 1974; Radiative Transfer within the Earth's Troposphere and Stratosphere: A Simplified Radiative Convective Model, J.A.S., Vol. 33, pp. 1330-1346.
18. Rodgers, C.D., and C.D. Walshaw, 1966; The computation of infrared cooling rate in planetary atmosphere. Quart. J. Roy. Meteor. Soc., 92, 67-92.
19. Slade, W.G., Jr., 1975; Infrared cooling of the atmosphere by the 9.6 micron band of ozone, SM thesis, Massachusetts Institute of Technology, Cambridge, MA 75 pp.
20. Tahnk, W.R. and R.E. Newell, 1975; Climatology and Energy Budget of the Northern Hemisphere Middle Stratosphere, Geofisca Internacional, 15(3), pp. 205-292.

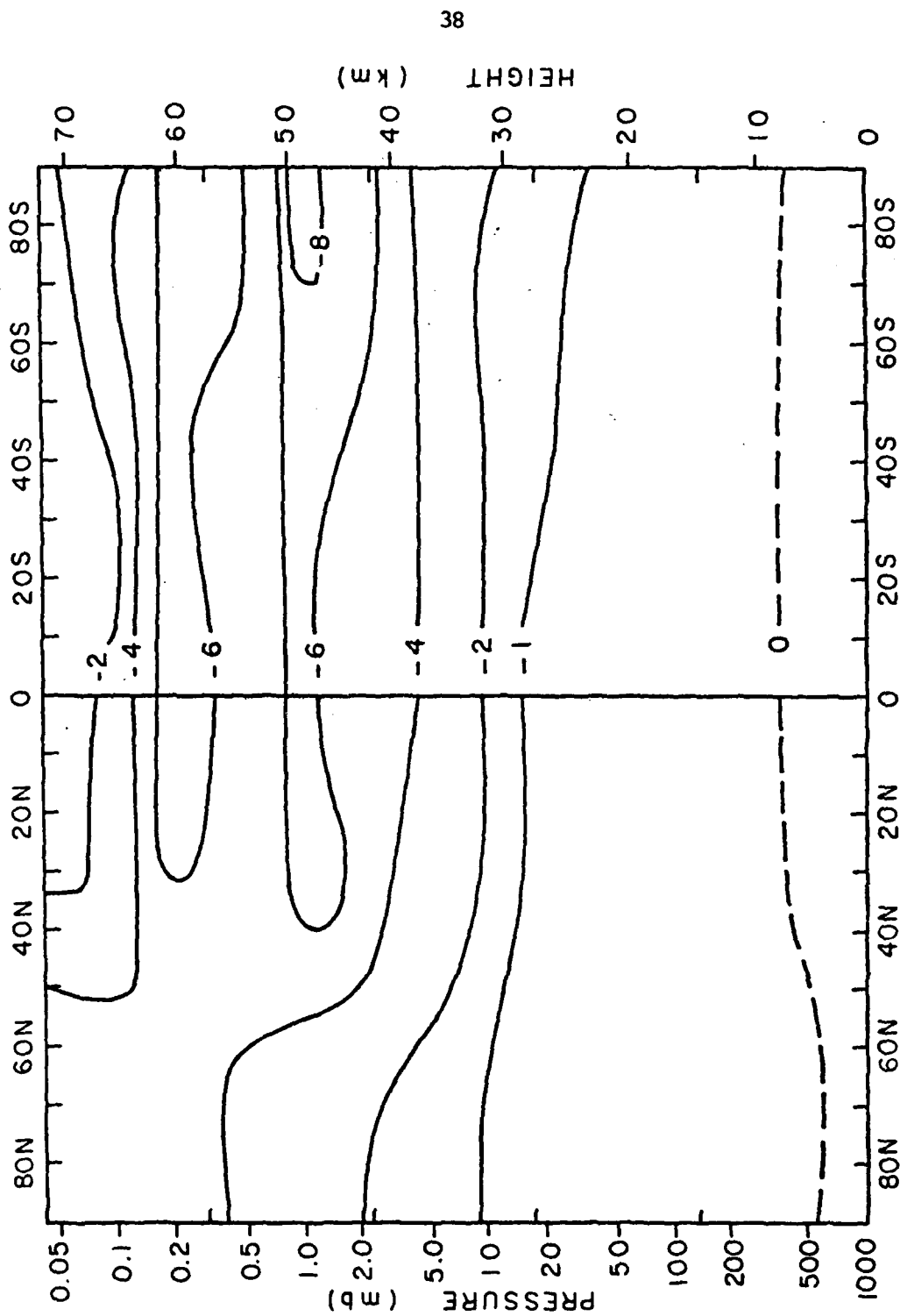


Figure 1: $15\mu\text{CO}_2$ cooling rate (degK/day) LATITUDE

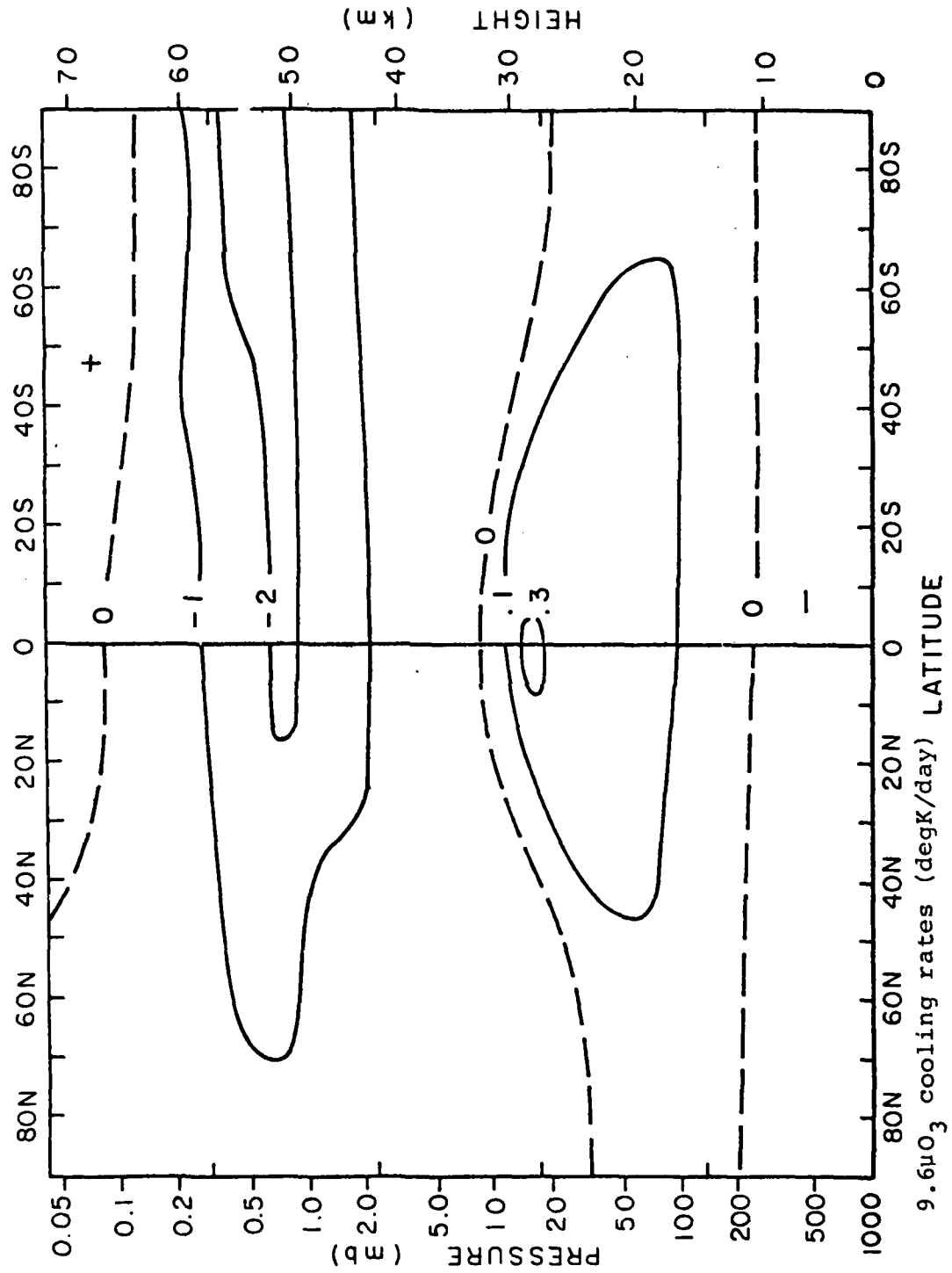


Figure 2: 9.6 μ O₃ cooling rates (degK/day) LATITUDE

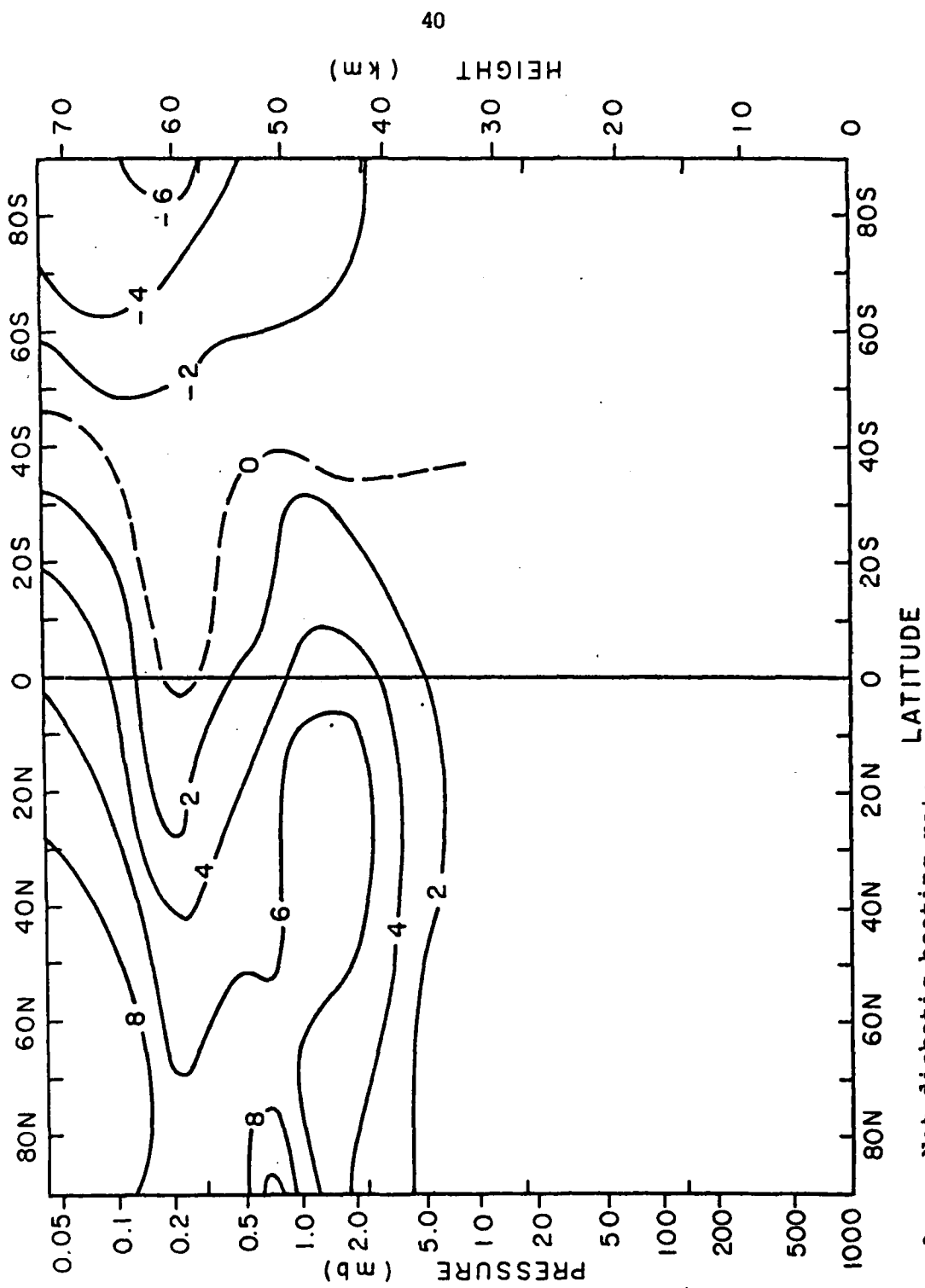


Figure 3: Net diabatic heating rates

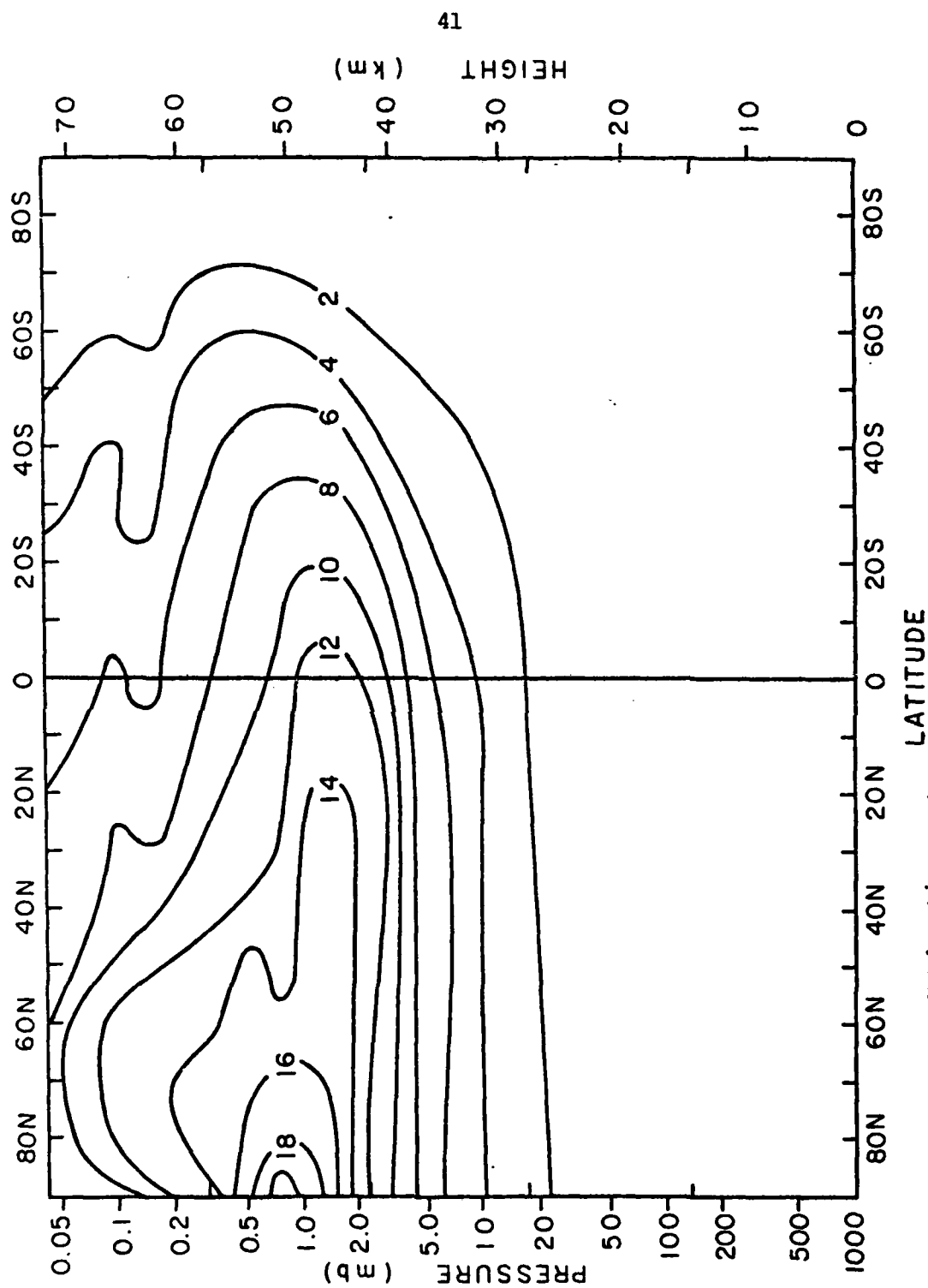


Figure 4: UV heating rates

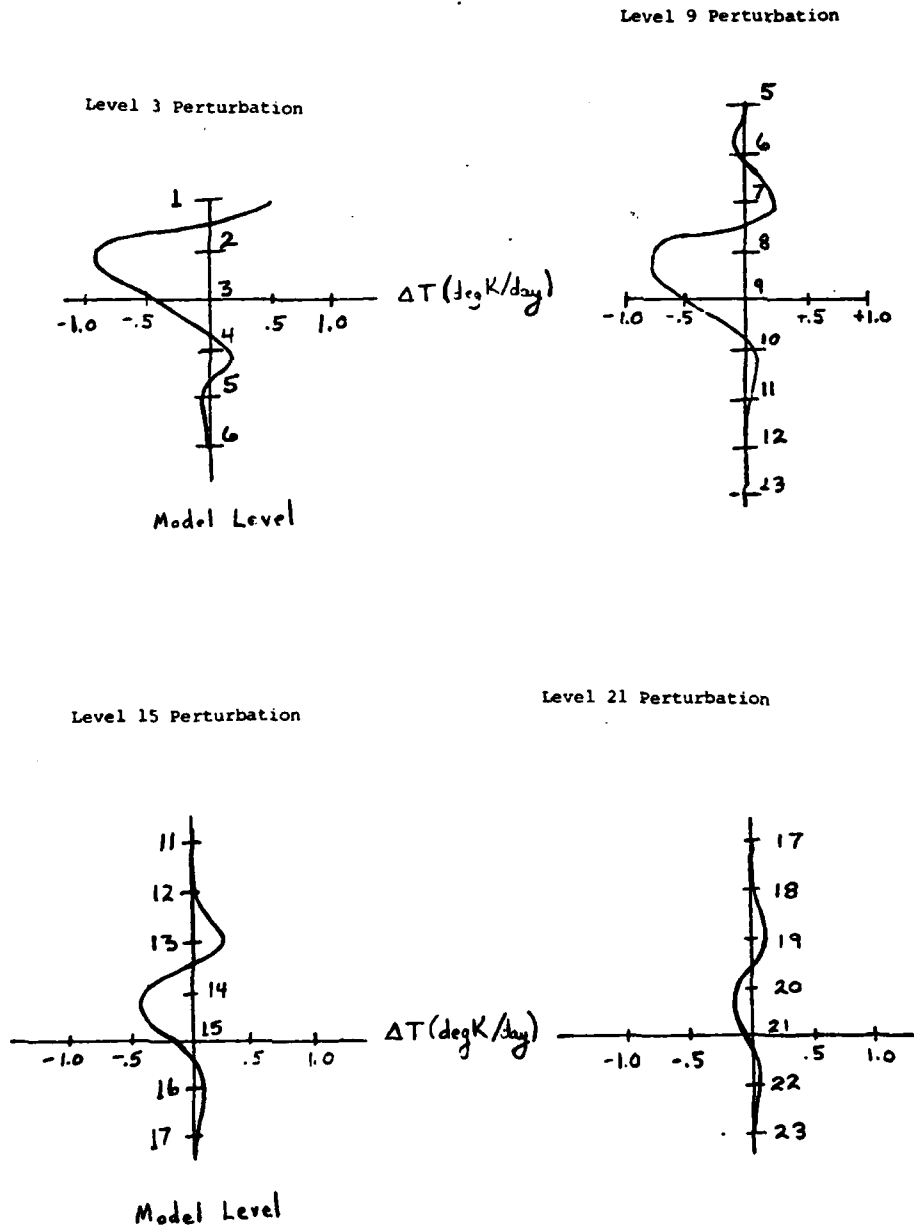


Figure 5: CO₂ cooling rate sensitivities to a 5°K temperature perturbation at selected model levels.

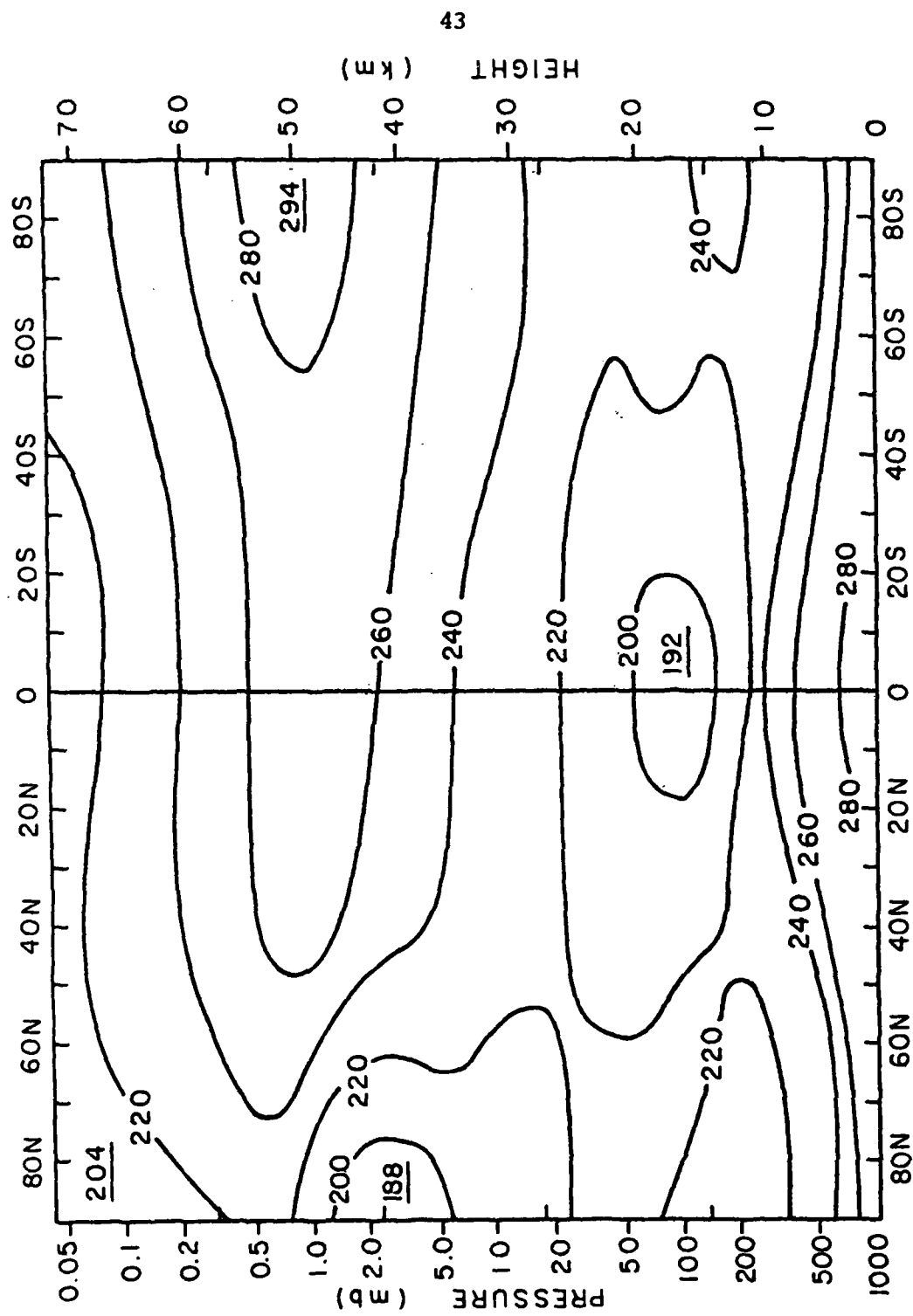


Figure 6: MIT GCM zonal averaged temperatures, Day 361, Run 34.

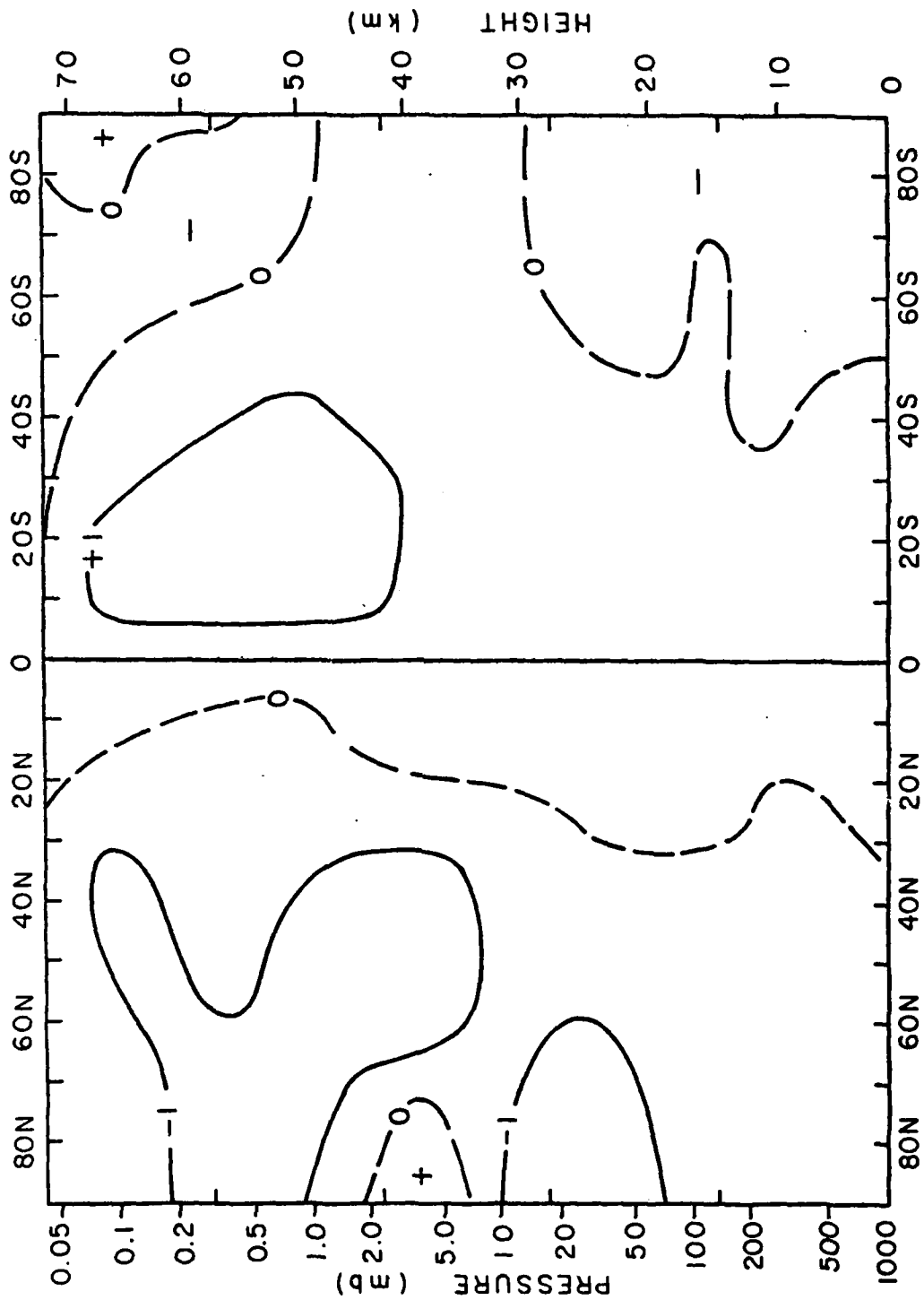


Figure 7: Zonal averaged net diabatic heating rates with Newtonian cooling, Day 361, Run 34.

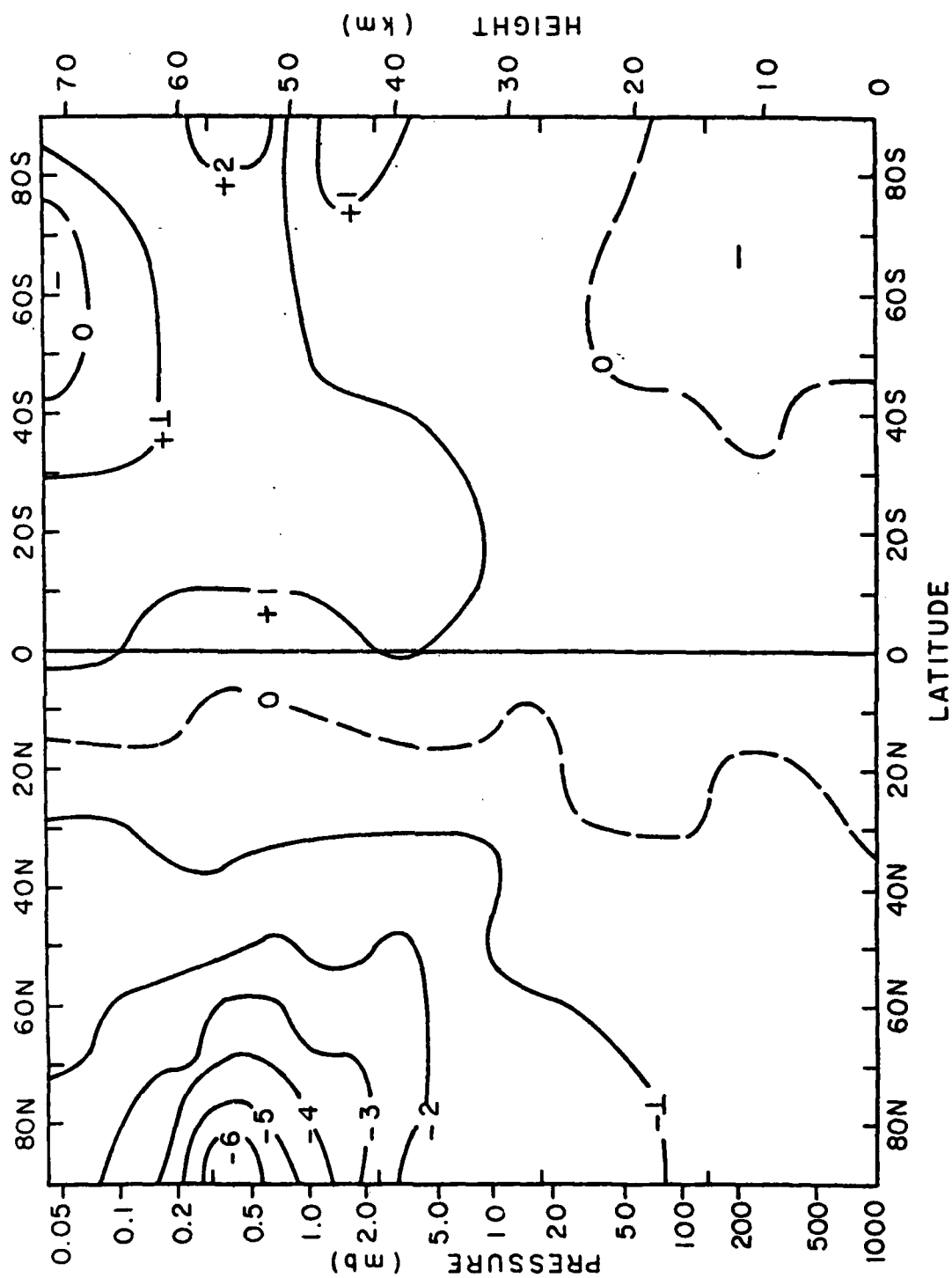


Figure 8: Zonal averaged net diabatic heating rates with band model cooling, Day 361, Run 34.

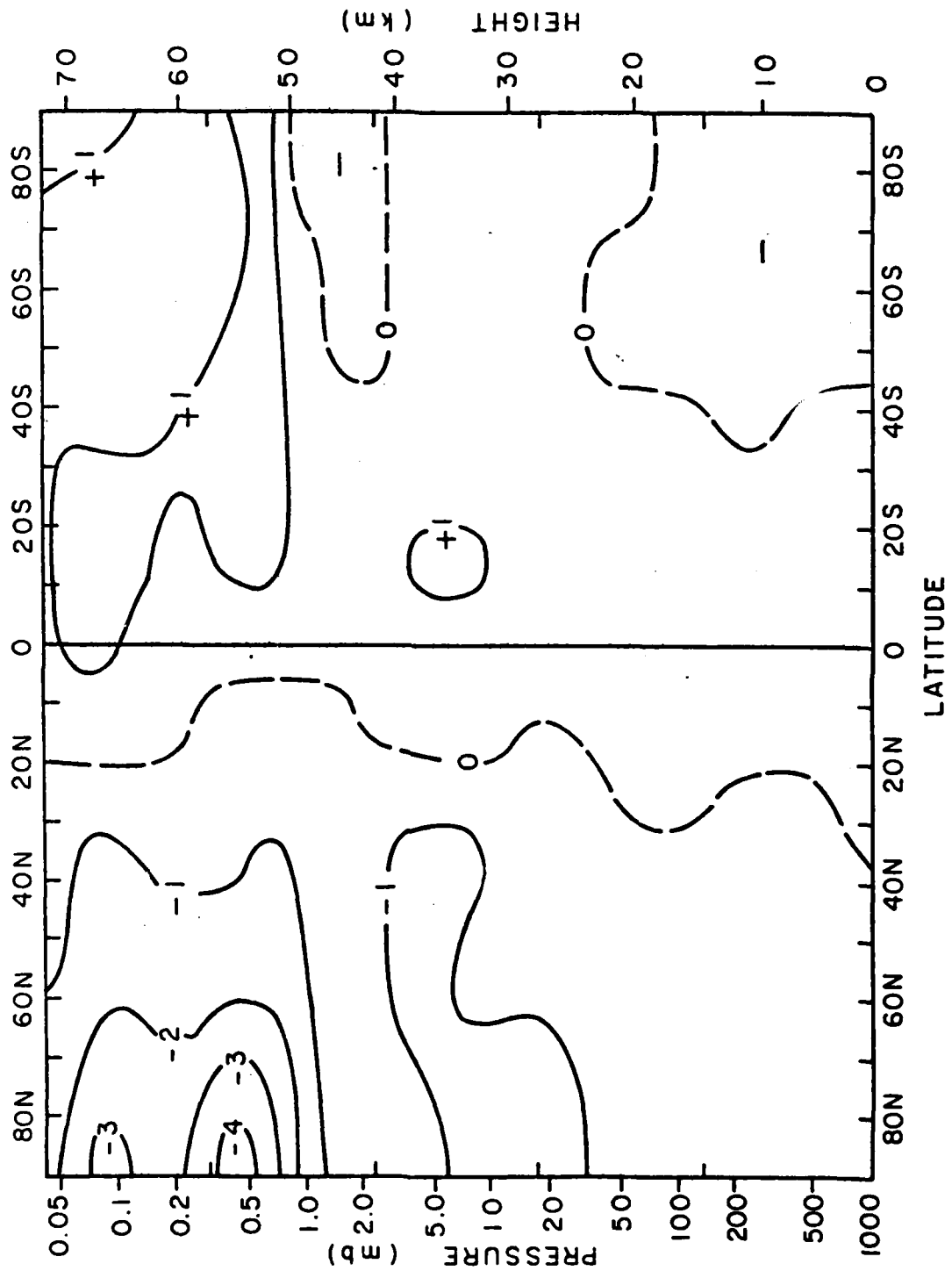


Figure 9: Zonal averaged net diabatic heating rates with adjusted cooling, Day 361, Run 34.

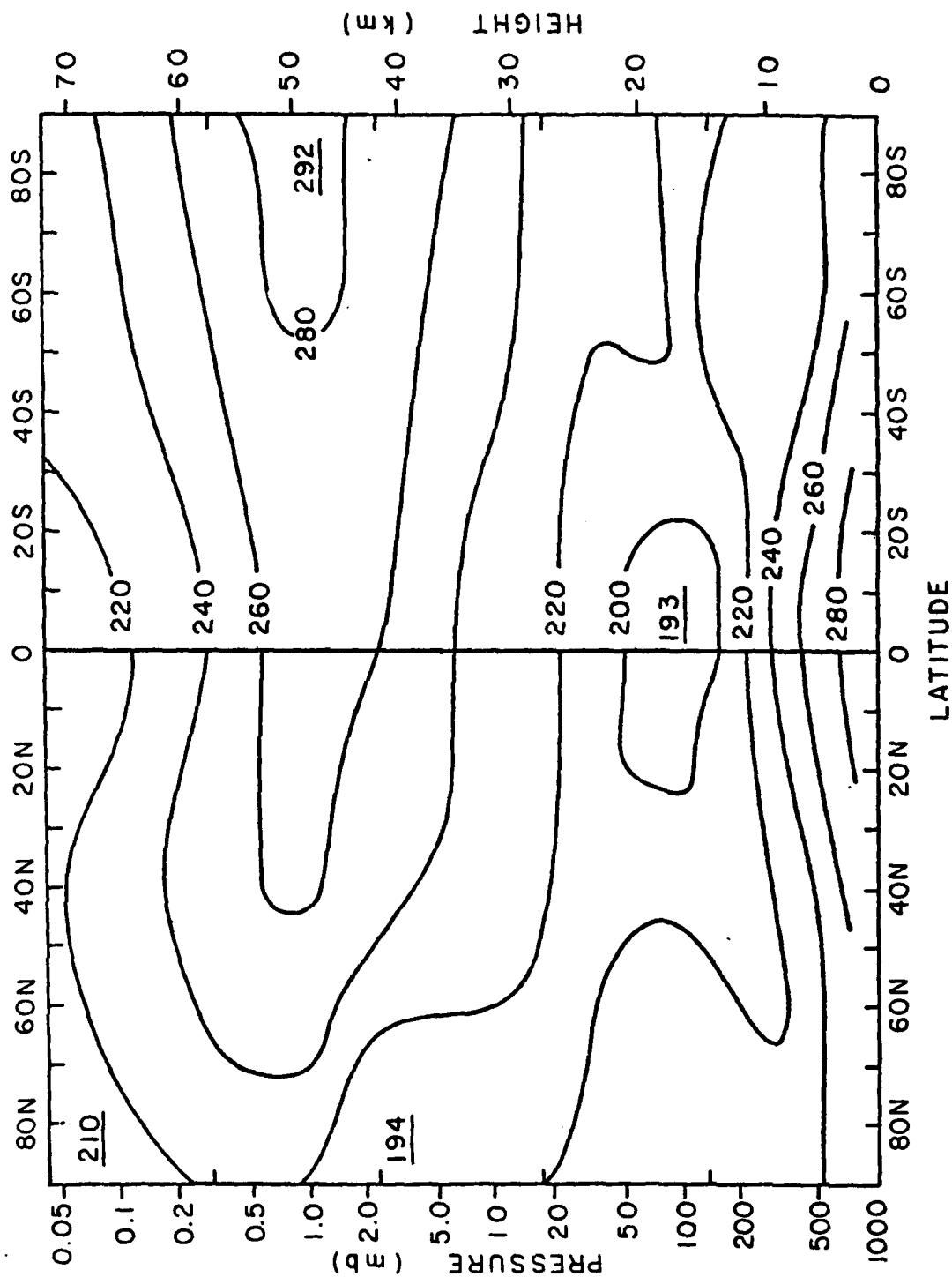


Figure 10: Zonal averaged temperature field after 5 days model integration with Newtonian cooling.

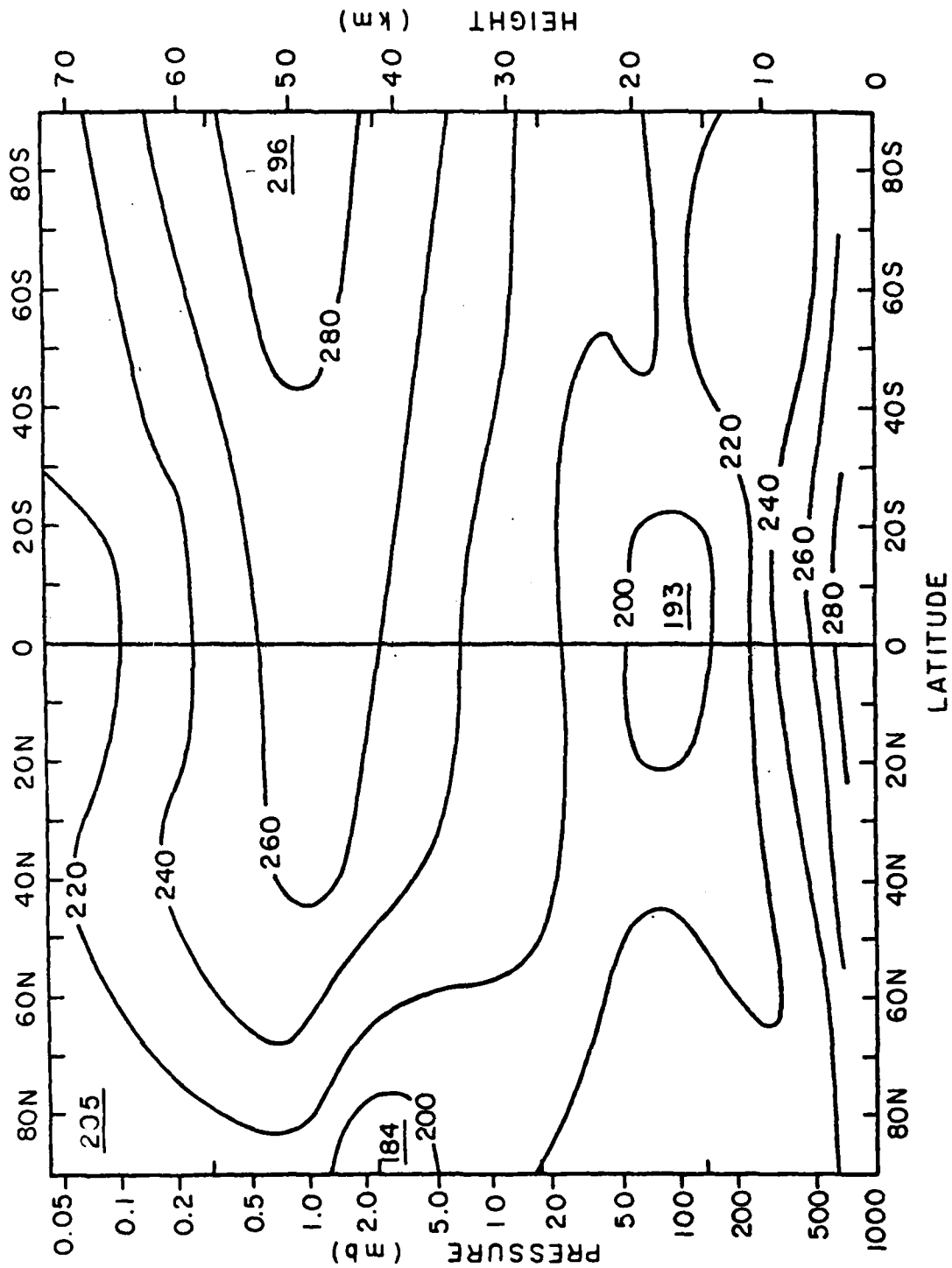


Figure 11: Zonal averaged temperature field after 5 days model integration with band model cooling.

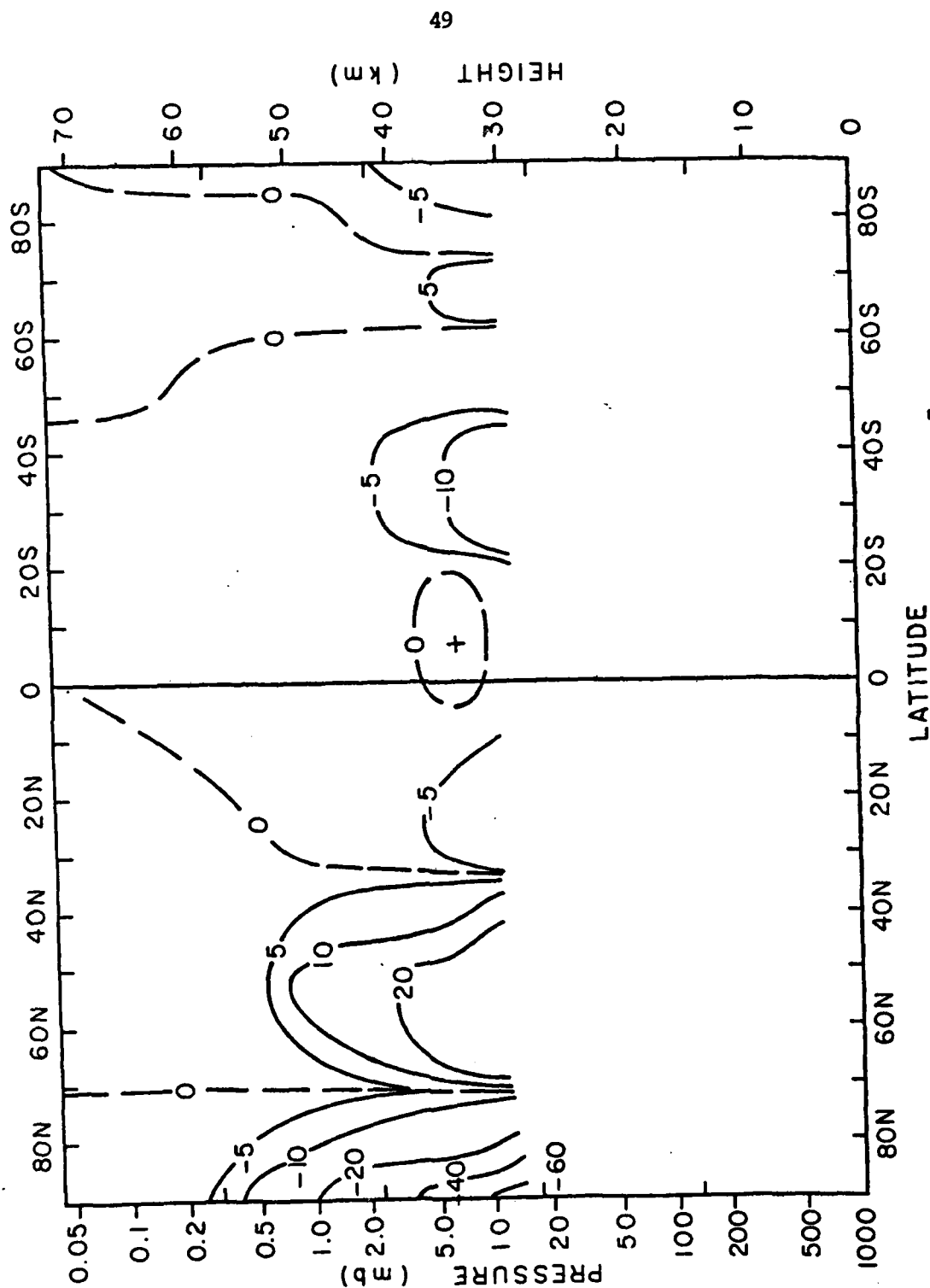


Figure 12: Zonal averaged vertical velocities (mb/sec $\times 10^7$) after 5 days model integration with Newtonian cooling

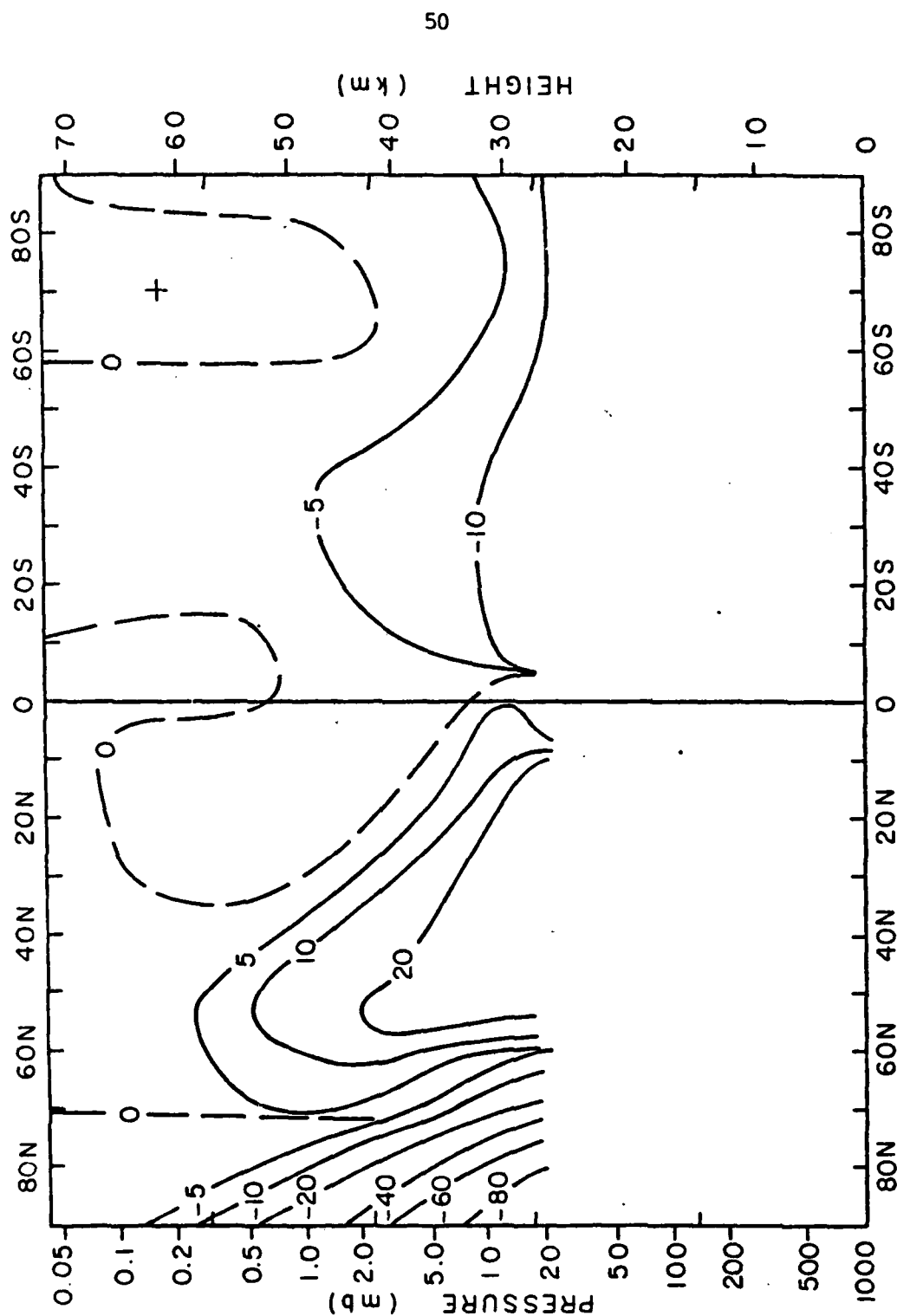


Figure 13: Zonal averaged vertical velocities (mb/sec $\times 10^7$) after 5 days model integration with band model

